Effect of Fabrication Process on Fracture Strength and Fatigue Life of Micromirrors Made from Single-Crystal Silicon

Yuanlin Xia*, Makoto Suzuki, Peidong Xue, Yoshikazu Hirai, Toshiyuki Tsuchiya

Department of Micro Engineering, Kyoto University, Kyoto, 615-8540, Japan

*Corresponding author: xia.yuanlin.35x@st.kyoto-u.ac.jp   Tel: +81 75 3833693

Abstract

We evaluated the effects of the source wafers [bare silicon (Si) and silicon-on-insulator (SOI)] and fabrication process on the fracture strength and fatigue life of micromirrors. The fracture strength of the Si-made micromirrors was 10 to 30% lower than that of the SOI-made ones. The decrease in strength was caused by the sidewall roughness. The low fracture strength shortened the fatigue life of the Si-made mirrors, but there is no significant difference in fatigue exponents between the Si- and SOI-made samples. By improving the fabrication process, we will be able to realize highly reliable Si-made micromirrors at a low cost.

Key words: Fabrication process; Fracture strength; Fatigue life; Torsional beam; Micromirror

1. Introduction

A micromirror, which is used to modulate reflected light, is one of the commonly used micro electro-mechanical systems (MEMS) devices [1]. A torsional micromirror device, which consists of a mirror plate and two torsional beams, is driven by electrostatic, electromagnetic, electrothermal, or piezoelectric actuation. For applications, such as light detection and ranging (LiDAR), and image projectors, the torsional micromirrors are always desired to be small, inexpensive, and highly reliable.

Fracture and fatigue properties of such torsional devices and structures at micro scales are always under the effects of the source wafer types and fabrication process. Typically, micromirrors are fabricated from a silicon-on-insulator (SOI) wafer since the torsional beams can be prepared easily with well-controlled geometry and dimensions. However, the high price of SOI wafers leads to a much higher micromirror production cost, which limits its application areas. Therefore, we have proposed a fabrication method using a bare silicon wafer, whose price is only one-tenth of that of the SOI wafer. The torsional beams are fabricated by the single-crystal silicon (SCS) reactive etch and metalization (SCREAM) process [2], in which the beam shape is formed by the combination of anisotropic (Bosch) and isotropic reactive ion etching (RIE) processes. Although the process cost has no significant difference, a sharp protrusion and a rough surface are formed on the bottom of the torsional beam during the isotropic RIE process, which may cause poor controllability of cross-sectional dimensions and reliability issues.

Under severe operating conditions such as high frequency (1 to 10 kHz), large number of cycles (>10^7 cycles), and large deflection angle (>20°) [3,4], high stress is generated on the torsional beams, which may cause failure. Extensive studies have shown the fracture and fatigue properties of silicon. The results indicate that the fracture strength of the SCS micro structure depends on the size [5], surface condition [6,7], and crystal orientation [7] of the test device. As for fatigue properties, it has been confirmed that the fatigue performance of SCS follows Paris law [8], similarly to those of brittle ceramics. However, most of these tests are conducted in tensile [9,10] and bending modes [11,12]. Only a few studies focused on the torsional mode [13].

To fabricate Si-made torsional beams that have high reliability comparable to that of SOI-made ones, a deep understanding of the fracture and fatigue properties of beam structures under torsional load is required to clarify where the fracture originates and what affects the reliability.

The purpose of this research is to realize high fracture strength and long fatigue life micromirrors with low cost. We compared the reliabilities of micromirrors made from Si and SOI wafers by fracture and fatigue tests under torsional load. Four types of micromirror with different dimensions were fabricated using both wafers. Torsional fracture and fatigue tests were conducted using a custom-made vibration test system. The effect of the fabrication process was evaluated.

2. Experiment

2.1. Design

Four types of micromirror named Types I, II, III, and IV were designed with different dimensions of mirror plates and torsional beams. Type I is the standard design, whereas Types II and III have the length of the torsional beam changed to modify fracture strength lower and higher, respectively. Type IV is designed to have a small beam width with the same resonant frequency. The dimensions of the mirror plate and torsional beam are shown in Table 1 and Fig. 1(a). The resonant frequency of the torsional mode is designed to be in the range from 500 to 1500 Hz so that the effect of attenuation caused by air damping is smaller at room temperature and atmospheric pressure. A fillet of 15 μm radius was formed at the root corner of the torsional beam to prevent stress concentration. To prevent damage of the torsional beam during fabrication, five support beams of 9 μm width were placed on each side, which was cut off by a laser trimming system (Hoya Candeo Optronics, HL-10L-SK) before the torsional test. All the mirrors were designed such that they were side by side on the same wafer surface.

2.2. Fabrication

In this work, a 4-inch SOI wafer (thicknesses: 15 μm Si, 1 μm SiO_2, and 400 μm Si) and a 4-inch Si wafer (400 μm thick) were used for the fabrication of SOI-made and Si-made micromirrors, respectively; both of them had a surface orientation of (100). The four types of SOI-made micromirror were named SOI-I, SOI-II, SOI-III, and SOI-IV, and the four types of Si-made micromirror were named Si-I, Si-II, Si-III, and Si-IV. Different fabrication processes were used for the SOI and Si wafers. The fabrication process of the SOI-made micromirrors is shown in Fig. 1(b) using a standard SOI-MEMS process, by which the dimension and shape of the torsional beam are accurately prepared. The details of the fabrication process were reported in our previous paper [14]. The SCREAM process using the Si wafer makes the cross-sectional shape and dimensions of the torsional beam difficult to control. The fabrication process of the Si-made micromirror is shown in Fig. 1(c). (1) A photoresist (Tokyo Ohka Kogyo, PMER P-CY1000) was spin-coated on the top surface and was patterned using a mask aligner (Suss Microtech, MA/BA8 Gen3). Beam structures were formed on the top surface by deep reactive ion etching (DRIE) using inductively coupled plasma (ICP) (Samco, RIEiPB800) at an etching rate of 130 nm/cycle. (2) The beam structures were released by isotropic etching. (3) An oxide film of 2 μm thickness was formed on the top surface by plasma-enhanced chemical vapor deposition (Sumitomo Precision Products, MPX-CVD). (4) The bottom surface was patterned under the same conditions as the top surface and was etched by another process at an etching rate of 3.5 μm/cycle. (5) A photoresist and fluorocarbon passivation film from DRIE were completely removed by oxygen plasma assisted ashing (Samco, FA-1). The oxide layer was etched by buffered hydrofluoric (BHF) acid.

2.3. Test method

Before the experiments, stress analysis using finite element analysis (FEA) was conducted by Autodesk Inventor Nastran (Autodesk Software) to estimate the maximum principal stress distribution. The models are shown in Figs. 2(a) and 2(b). The shape and dimensions of the torsional beam model were chosen from the measurement of the fabricated micromirrors. The x, y, and z axes of the model correspond to the crystal orientations of [110], [$\bar{1}$10], and [001], respectively. Table 2 shows the parameters used for the simulation [15]. For the constraints of stress analysis, one end of the torsional beam was defined as an anchor, whereas the other end was rotated around the neutral axis of the torsional beam.

Because it is difficult to apply pure torsional deformation, all tests were conducted using resonant vibrations on a custom-made system under laboratory air (25°C, ~50% RH), in which the vibration was applied by a piezoelectric actuator (NTK Ceratec, PAC166J) and the tilting angle amplitude was recorded by a position sensitive detector (PSD, Hamamatsu Photonics, S3270-01) [14]. The test procedure was as follows. First, a frequency sweep was performed to find the torsional resonant frequency. The actuation was small during the sweep so as not to affect the strength measurement. Next, the actuation frequency was set to its torsional resonance, and amplitude was gradually increased while maintaining the resonance. Finally, the maximum amplitude as the mirror device broke was recorded. A resonant frequency shift (around 0.5 to 1 Hz) [16] was observed during the torsional fracture test, which occurred as a sudden increase in the angle amplitude as the applied voltage increased. Moreover, owing to the high Q-factor (around

1000), even a small change of 0.1 Hz causes an angle amplitude fluctuation of more than 1°. Therefore, the driving frequency should be controlled with the resolution of 0.01 Hz. The entire test procedure should be conducted in a small cycle (less than 10^5) to prevent significant fatigue effects on the fracture strength [17,18]. At least five samples were tested under each condition. The vibration applied by the actuator may lead to not only torsional but also horizontal or vertical bending deformations. However, the bending deformation is small compared to the torsional one. Thus the simulation and analysis are conducted by assuming a pure torsional deformation. The torsional fracture strength τ_f was calculated from the maximum angle amplitude θ_{max}:

$$\tau_f = \frac{\beta b G}{\alpha l}\theta_{\max}, \tag{1}$$

where α and β are constants depending on the aspect ratio of the cross section. α and β are 0.208 and 0.141 for the square cross section (types I, II, and III, b/a=1) and 0.246 and 0.229 for type IV (b/a=2), respectively. G is the shear modulus. However, since the fillet at the root corner of the torsional beam may affect the resonant frequency, the equivalent length (l_e) obtained from the measured resonant frequency was used for the calculation of τ_f by the following equation:

$$f_t = \frac{1}{2\pi}\sqrt{\frac{2\beta a^3 b G}{j l_e}}, \tag{2}$$

where j is the moment of inertia about the neutral axis of the torsional beam. $j=1/12M(W^2+H^2)+M(d^2+e^2)$, where M is the mass of the mirror plate. Angle amplitude was converted to stress amplitude by substituting (2) to (1). The fracture strength τ_f was

$$\tau_f = \frac{2\pi^2 j}{\alpha}\cdot\frac{f_t^2\theta_{\max}}{a^3}. \tag{3}$$

In the fatigue test, frequency sweep was conducted first to find the resonant frequency. Next, the amplitude was increased to a set stress level. Three levels of 80, 85, and 90% of the average maximum fracture angle obtained in the fracture test were selected. Three samples were performed at each level. Then, the resonance at the amplitude level was kept until failure. Finally, the number of cycles to fatigue was calculated as the product of the resonant frequency and the time to failure. The ramping cycle required to reach the amplitude level was assumed to be sufficiently smaller than the cycle to failure. After the test, the fracture surfaces were observed using a field emission scanning electron microscope (FESEM, Hitachi, SU-8020). The sidewall roughness of the torsional beam was measured using a 3D laser microscope (Olympus, OLS4000-SAT).

3. Results

3.1 Fabrication

The fabricated torsional beams of SOI-I and Si-I are shown in Figs. 3(a) and 3(e), respectively. All sides of the SOI-made torsional beam have a smooth surface with a square cross section [Figs. 3(c) and 3(d)], whereas vertical striations are observed on the sidewall of the Si-made torsional beam [Figs. 3(e)]. Figures. 3(b) and 3(f) show the surface profiles measured by the laser microscope. The arithmetic average roughness *Ra* was measured along the red line at the center of the sidewall where the expected maximum stress was generated. The roughness of the Si-made sample is four times larger than that of the SOI-made sample. A sharp protrusion and a rough surface appear at the bottom of the Si-I torsional beam as predicted, whereas that of Si-IV almost disappears owing to a relatively longer etching time for a small beam width, as shown in Figs. 3(g) and 3(h).

3.2 Simulation

Figs. 2(c)−2(f) show the distribution of the maximum principal stress of the torsional beam. Types I, II, and III have similar stress distributions. The contour plots used 80% (blue, 1.53 to 2.42 GPa for different samples) to 100% (red) of the maximum stress value as the range of the color scale to observe the local stress concentration. The point where the maximum stress occurs is indicated by a white arrow. The maximum principal stresses of Si and SOI have similar distributions, which are symmetric around the beam axis passing through the center line of the sidewall and show a good agreement with Namazu et al.'s report [19]. A difference was found between types I−III and type IV. As shown in the cross section plots where the maximum principal stress exsits [insets of Figs. 2(c)-2(f)], for types I, II, and III, 90% (green) of the maximum principal stress was generated at the bottom of the torsional beam, whereas only 80% was found for type IV.

3.3 Frequency response

Table 3 shows the resonant frequencies of types I and IV. The resonant frequencies of the Si-made mirrors are 25 to 30% higher than those of the SOI-made ones except for type IV. The higher resonant frequencies of the Si-I, Si-II, and Si-III mirrors are caused by the sharp protrusion at the bottom of the torsional beam, which increases the cross-sectional area and thus gives a higher stiffness. The sharp protrusion effect on frequency may be reduced or eliminated by decreasing the thickness b of the torsional beam. The small or even the absence of sharp protrusion of Si-IV reduces its difference in resonant frequency with SOI-IV to less than 5%. Typical frequency responses at a small angle of types I and IV are shown in Fig. 4. The Q-factors were calculated from the full width at half maximum Δf of the resonant peak:

$$Q = \frac{f_t}{\Delta f}. \tag{4}$$

The measured Q-factors ranged from 800 to 1000, which indicates a smaller range of resonant frequencies and is more stable for frequency selection.

3.4 Fracture strength

For the torsional fracture strength directly calculated from the theoretical Eq. (3) (τ_f), the effects of the shape and anisotropy of actual Si beams on calculated results are not considered, thus, we have compared τ_f with simulation results (τ_{sim}) to evaluate the accuracy of Eq. (3) for stress estimation. The simulation results τ_{sim} are the maximum torsional stress at the center part of the sidewall, which is obtained by setting the deformation angle in the simulation to be the same as the angle amplitude in the fracture test at failure (shown as θ in Table 3). All the τ_f values of the SOI-made samples are lower than τ_{sim}, whereas those τ_f of the Si-I, Si-II, and Si-III are similar to τ_{sim}, as shown in Table 3. In the simulation, the setting parameters have defined the anisotropy of silicon, but Eq. (3) for fracture strength measurements is only for an isotropic material, which causes the difference between τ_{sim} and τ_f. As a result, a τ_{sim}/τ_f ratio of around 1.1 is obtained for the SOI-made samples. However, for the measurements of Si-I, Si-II, and Si-III, the sharp protrusion at the bottom of the torsional beam may change the actual torsional constants α in Eq. (3), which causes a larger τ_f and results to a similar value to τ_{sim} with the τ_{sim}/τ_f ratio of around 1. The results suggest that τ_f is acceptable and reliable for stress estimation, and the following description and discussion are based on τ_f.

The strength of silicon-based microstructure is dominated by the local stress. When the maximum stress reach the intrinsic strength of silicon, the microstructure will fail. The torsional angle at failure is related to the maximum stress of torsional beam. Thus we can compare the fracture strength by the difference of the tilting angle. No matter for Si-I, Si-II, and Si-III that have the sharp protrusion at the bottom of the torsional beam, or for Si-IV that has only small or even no sharp protrusion, all the fracture strengths τ_f of the Si-made mirrors are about 10 to 30% lower than those of the SOI-made ones. The fracture strength values are plotted against the resonant frequencies in Fig. 5. The high roughness of the sidewall of the Si-made beam increases the uncertainty of crack initiation, which causes the strength scattering of the Si-made samples to be larger than that of the SOI-made samples. Our other set of work, in which Si-IV samples with the thickness *b* of 14 μm are tested, shows a lower resonant frequency (455.7 Hz) but higher angle amplitude (20.49°) at fracture. However, the fracture strength of Si beam remains lower (2.11 GPa) than that of SOI. It indicates that the thickness of the torsional beam does not affect the fracture strength significantly. The same conclusion also applies to other types.

The fracture surfaces of the SOI-I and Si-I mirrors are shown in Figs. 6(a) and 6(c). The other three types show fracture surfaces similar to that of type I. The fracture initiates near the center line of the sidewall where the maximum stress exists, extending up or down along the (111) planes that has the lowest surface energy in single crystal silicon. Then, upon application of an axial torsional load, the cracks change their direction of propagation to helical cracking, causing an irregular fracture surface. Similar observation was reported in Ref. [20]. Several beams at the opposite side of mirrors have a flat fracture surface along the (111) plane [Figs. 6(b) and 6(d)], which is like a tensile fracture similar to that in our previous study [21]. This result indicates that the failure of the mirror started from one of the torsional beams; then, the mirror plate fell, pulling the other torsional beam and producing the fracture surface similar to the tensile testing. Fracture does not initiate from the sharp protrusion where fatal flaws are easily introduced, leading to failure of the entire structure. As already shown in the stress analysis, even at a high torsional angle amplitude, the stress distribution on the bottom side is only 80 to 90% of the maximum principal stress; thus, failure will not start at the sharp protrusion.

3.5 Fatigue test

Fatigue tests of types I and IV of Si- and SOI-made mirrors were conducted. The fatigue lives of all the tested types show large scatterings as summarized in Fig. 8. None of the samples failed during ramping and all of them showed a delayed fracture with a fatigue life *n* from 1.74×10^5 to 5.62×10^7 cycles. The results show that when the angle amplitude decreases, the fatigue life becomes longer. All the samples show similar fracture surfaces in the torsional fracture test as shown in Fig. 6. The waveform at the moment of fracture is shown in Fig. 7(a). The fracture occurs as the amplitude increases. No change in the waveform is observed before the failure; thus, external effects such as oscillation instability and electric noise pulses are excluded. The angle amplitude during the entire test is shown in Fig. 7(b). No clear change in the angle amplitude is observed before the drop, in which the failure of the mirror is evaluated to be caused by a normal fatigue crack growth. A shift up to 0.5 Hz in resonant frequencies was also found during the fatigue test, which resulted in a change in angular amplitude of up to 0.5° to 1°. Although this shift was corrected when we found it, it would more or less cause measurement errors of fatigue life. Therefore, a real-time monitoring and feedback adjustment of resonant frequency is necessary in future work.

4. Discussion

4.1. Effect of source wafer and fabrication process on torsional strength

The different beam shapes and dimensions resulted from the different source wafers, and fabrication processes are considered to cause the torsional strength differences. We deduced that the sharp protrusion at the bottom of the Si-made beam structure may easily generate cracks and decrease the strength of the Si-made micromirrors. However, the observation of the fracture surface indicates that cracks do not initiate from the bottom surface. Instead, the fracture origin is found to locate around the center part of the sidewall for all the samples. Thus, we conclude that the roughness of the beam sidewall shown in Fig. 3(e) is the main reason for the low fracture strength of the Si-made micromirrors. Regarding the stress distribution in the FEA analysis, the maximum stress exactly located at the center line of the sidewall where a large roughness exists, which causes stress concentration at the center parts and accelerates the crack propagation. Regarding the surface roughness as an initial flaw with size c on the beam surface, the fracture stress σ_f is calculated on the basis of Griffith's theory as

$$\sigma_f = \sqrt{\frac{2\gamma E}{\pi c}}. \tag{5}$$

where γ is surface energy and E is Young's modulus of silicon. By employing the roughness values as crack length c, we found that the theoretical σ_f of the SOI-made mirror is twice as large as that of the Si-made one, which indicates that high roughness decreases strength.

The formation of vertical striations with high roughness is considered to be produced during deep reactive ion etching owing to the use of different photoresists and exposure methods during the etching process. The different types (THMR-iP1800 [14] for SOI and CY-1000 for Si) and thicknesses (0.95 μm for SOI and 7 μm for Si) of photoresists may change the etching condition to silicon. Moreover, the lithography of the silicon wafer using contact exposure cannot provide a well-patterned smoothness and morphological uniformity at the edge (accuracy<0.25 μm), whereas the SOI wafers were patterned by projection exposure (Nikon NSR2205i11D) with a 5:1 reduction ratio to provide high accuracy (<70 nm) of the side edge. During the Bosch process for Si, the edge roughness of the photoresist pattern is transferred to the etched silicon and is gradually enlarged to form the vertical striations. If the etching process is properly improved and the sidewall roughness is reduced, the strength of the Si-made torsional beams will become comparable to that of the SOI-made ones. Moreover, a protective coating [21] or surface smoothing by hydrogen annealing [7] is also a concise way to improve the roughness of the sidewall.

4.2 Fatigue properties

The stress–life relationship obtained from the fatigue test was plotted as a S–N curve for high-cycle repetition around 10^5 to 10^8. Under a constant stress amplitude, the applied stress amplitude σ and the fatigue life n (in cycles) satisfy the relationship $\sigma^N \cdot n = const$ [22], where N is the crack growth exponent, which indicates the degree of subcritical crack propagation against the stress intensity factor based on Paris law [23, 24]. The N is around 10 to 50 in the presence of some brittle materials [25]. Fig. 8 shows the fitted S–N lines. The dashed lines are drawn as the average fracture strength connected with S–N lines. Despite the variety of configurations and testing conditions, all these curves show a shape similar to that in our previous reports [8,12].

For type I, no significant difference in N was found between the Si-made and SOI-made mirrors. The similar N of around 41.7–46.0 implies that the fatigue behaviors of types I and IV depend on an identical or similar crack growth mechanism [8]. The fitted line of SOI-I shows a ~0.18 GPa shift in the stress amplitude axis from Si-I, which corresponds to an extension of the fatigue life by ~10^2 in the fatigue cycle axis. The low initial strength caused by the high surface roughness is considered to be the reason for the shorter fatigue life of the Si-made mirrors. The mechanical defects (that is roughness in our research) are detrimental to fracture strength and fatigue life was also reported previously [26,27]. The same explanation can also be used for type IV corresponding to ~10^4 fatigue cycle shortening, whose N values for Si and SOI samples are also similar.

With regard to the difference between types I and IV, the *N* value of type IV is nearly 25% lower than that of type I. This decrease is found for both Si- and SOI-made mirrors. The reason is yet unknown, but some possibilities such as local stress concentration due to different cross-sectional shapes are considered. Moreover, the *N* values of the torsional mode in this work and Ref. [13] are larger than those of the bending and tensile modes reported in Refs. [10-12], which are summarized in Table 4. The different fracture modes and fracture origins may be the reason for the different *N* values. In bending and tensile tests, cracks generally initiate at the corner edge, whereas in the torsional test, the fracture origin is at the center line along the beam sidewall.

5. Conclusion

In this work, we proposed a silicon-wafer-based fabrication method for low-cost torsional micromirror devices. To evaluate the effect of the fabrication process on the reliability of the torsional beams, four types of micromirror were fabricated from silicon and SOI wafer. In the torsional fracture and fatigue tests, fractures of both Si and SOI samples initiated near the center line of the sidewall where the maximum stress occurs, which is consistent with the simulation results. The sharp protrusion existing on the bottom of the Si-made torsional beam enhanced the stiffness and caused a high resonant frequency compared with the SOI-made mirrors. However, the high roughness induced by DRIE on the sidewall of the Si-made torsional beam causes a lower fracture strength (10 to 30% decrease), a larger strength scattering, and a shorter fatigue life (10^2 to 10^4 cycles shortening) compared with those of the SOI-made ones. No significant difference in fatigue exponents *N* was found between the Si-made and SOI-made mirrors, indicating similar crack growth mechanisms. These findings suggested that if the surface is well smoothed by improving the etching process, highly reliable Si-made MEMS mirrors comparable to SOI-made ones will be realized at a low cost.

Acknowledgments

The authors are grateful to Mr. Ishikawa, Kyoto University, for the observation with FESEM. Part of the fabrication and characterization work was supported by the Nanotechnology Platform Project at Kyoto University.

Reference

[1] R. Maeda, J.J. Tsaur, S.H. Lee, M. Ichiki, Piezoelectric micro actuator devices, J. Electroceram. 12 (2004) 89-100.

[2] K.A. Shaw, Z. Lisa, N.C. MacDonald, SCREAM I: a single mask, single-crystal silicon, reactive ion etching process for microelectromechanical structures, Sensor. Actuat. A. 40 (1994) 63-70.

[3] A. Arslan, D. Brown, W.O. Davis, S. Holmstrom, S.K. Gokce, H. Urey, Comb-Actuated Resonant Torsional Microscanner With Mechanical Amplification, J. Microelectromech. Syst. 19 (2010) 936-943.

[4] S.T.S. Holmstrom, U. Baran, H. Urey, MEMS Laser Scanners: A Review, J. Microelectromech. Syst. 23 (2014) 259-275.

[5] T. Namazu, Y. Isono, T. Tanaka, Evaluation of size effect on mechanical properties of single crystal silicon by nanoscale bending test using AFM, J. Microelectromech. Syst. 9 (2000) 450-459.

[6] S. Izumi, Y. Kubodera, S. Sakai, H. Miyajima, K. Murakami, T. Isokawa, Influence of ICP Etching Damage on the Brittle-Fracture Strength of Single-Crystal Silicon, J. Soc. Mater. Sci. 56 (2007) 920-925.

[7] R. Hajika, S. Yoshida, Y. Kanamori, M. Esashi, S. Tanaka, An investigation of the mechanical strengthening effect of hydrogen anneal for silicon torsion bar, Journal of Micromechanics and Microengineering. 24 (2007) 105014,

[8] S. Kamiya, T. Tsuchiya, T. Ikehara, K. Sato, T. Ando, T. Namazu, CROSS comparison of fatigue lifetime testing on silicon thin film specimens, Proc. IEEE. Int. Conf. Micro. Electro. Mech. Syst. (2011) 404-407.

[9] T. Ando, M. Shikida, K. Sato, Tensile-mode fatigue testing of silicon films as structural materials for MEMS. Sensor. Actuat. A. Phys. 93 (2001) 70-75.

[10] T. Tsuchiya, Y. Yamaji, K. Sugano, O. Tabata, Tensile and tensile-mode fatigue testing of microscale specimens in constant humidity environment. Exp. Mech. 50 (2010) 509-516.

[11] D. H. Alsem, O. N. Pierron, E. A. Stach, C. L. Muhlstein, R. O. Ritchie, Mechanisms for fatigue of micron-scale silicon structural films. Adv. Eng. Mater. 9 (2007) 15-30.

[12] T. Ikehara, T. Tsuchiya, Low-cycle to ultrahigh-cycle fatigue lifetime measurement of single-crystal-silicon specimens using a microresonator test device, J. Microelectromech. Syst. 21 (2012) 830-839,

[13] I. Satoshi, K. Masayuki, S. Shinsuke, U. Yuzuru, S. Atsushi, Proposal of a Reliability-Based Design Method for Static and Fatigue Strength of MEMS Micromirror, J. Soc. Mater. Sci. 55 (2006) 290-294.

[14] W. Zhang, K. Obitani, Y. Hirai, T. Tsuchiya, O. Tabata, Fracture strength of silicon torsional mirror resonators fully coated with submicrometer-thick PECVD DLC film. Sensors and Actuators A: Physical, 286 (2019) 28-34.

[15] A. Matthew, D. William Nix, W. Thomas, What is the Young's Modulus of Silicon? J. Microelectromech. Syst. 10 (2010) 229-238.

[16] L.G.W. Tvedt, D.S. Nguyen, E. Halvorsen. Nonlinear behavior of an electrostatic energy harvester under wide-and narrowband excitation. J. Microelectromech. Syst. 19 (2010) 305-316.

[17] A. Wolter, H. Schenk, H. Korth, H. Lakner, Torsional stress, fatigue and fracture strength in silicon hinges of a micro scanning mirror, Proc. SPIE. Int. Soc. Opt. Eng. 5343 (2003) 176–185.

[18] O.N. Pierron, C.L. Muhlstein, The critical role of environment in fatigue damage accumulation in deep-reactive ion-etched single-crystal silicon structural films, J. Microelectromech. Syst. 15 (2006) 111-119.
[19] T. Namazu, H. Yamagiwa, S. Inoue, Tension-torsion combined loading test equipment for a minute beam specimen, J. Eng. Mater. Technol. 135 (2013) 011004.
[20] A. Gryguć, S.B. Behravesh, H. Jahed, M. Wells, B. Williams, X. Su, Multiaxial fatigue and cracking orientation of forged AZ80 magnesium alloy. Procedia Structural Integrity, 25 (2020) 486-495.
[21] Y. Xia, Y. Hirai, T. Tsuchiya, Fracture behavior of single-crystal silicon microstructure coated with stepwise bias-graded a-C: H film. Surf. Coat. Technol. (2020) 126559.
[22] A.G. Evans, E.R. Fuller, Crack propagation in ceramic materials under cyclic loading conditions. Metall. Trans. 5 (1974) 27-33.
[23] P. Paris, F. Erdogan, A critical analysis of crack propagation laws. (1963).
[24] A.G. Evans, H. Johnson, The fracture stress and its dependence on slow crack growth. J. Mater. Sci. 10 (1975) 214-222.
[25] A.G. Evans, A method for evaluating the time-dependent failure characteristics of brittle materials and its application to polycrystalline alumina. J. Mater. Sci. 7 (1972) 1137-1146.
[26] T. Ikehara, T. Tsuchiya, Measurement of anisotropic fatigue life in micrometre-scale single-crystal silicon specimens, Micro. Nano. Lett. 5 (2010), 49-52.
[27] A. Gryguc, S.B. Behravesh, H. Jahed, M. Wells, B. Williams, R. Gruber, . Effect of thermomechanical processing defects on fatigue and fracture behaviour of forged magnesium. Frattura ed Integrità Strutturale, 15 (2021) 213-227.

Figure captions

Fig. 1 Fabrication of micromirrors. (a) Schematic of torsional microstructure. (b) Fabrication process of SOI-made micromirror. (c) Fabrication process of Si-made micromirror. (d) micromirrors with support and torsional beams.

Fig. 2 Simulation results. (a),(b) 3D models of SOI and Si torsional beams used for FEA. (c)−(f) Maximum principal stress distributions of SOI and Si torsional beam. Inserts are the cross section at the middle of the torsional beam. Left: entire models. Right: magnified views of beam part (red dashed line in entire model).

Fig. 3 Microstructure of torsional beam. (a)−(d) SOI-made torsional beams. (e)−(h) Si-made torsional beams. (a) & (e) Entire structure of torsional beam observed at a tilt angle of 30°. (b) & (f) 3D measuring structure. (c) & (g) Cross section of type I. (d) & (h) Cross section of type IV.

Fig. 4 Typical frequency response of types I and IV for SOI- and Si-made torsional micromirrors.

Fig. 5 Fracture strength against resonant frequency.

Fig. 6 Typical fracture surfaces of torsional beam for type I. (a), (b) Torsional beams of SOI-I. (c), (d) Torsional beams of Si-I.

Fig. 7 (a) Waveform at fracture for Si-I in the enlarged time scale of microseconds. The time at fracture is plotted as 0. (b) Amplitude response of SOI-I and Si-I in entire fatigue test.

Fig. 8 Measured stress−life behavior of SOI and Si samples. Dashed lines are drawn as the average fracture strength. Solid lines indicate fitted curves based on Paris law.

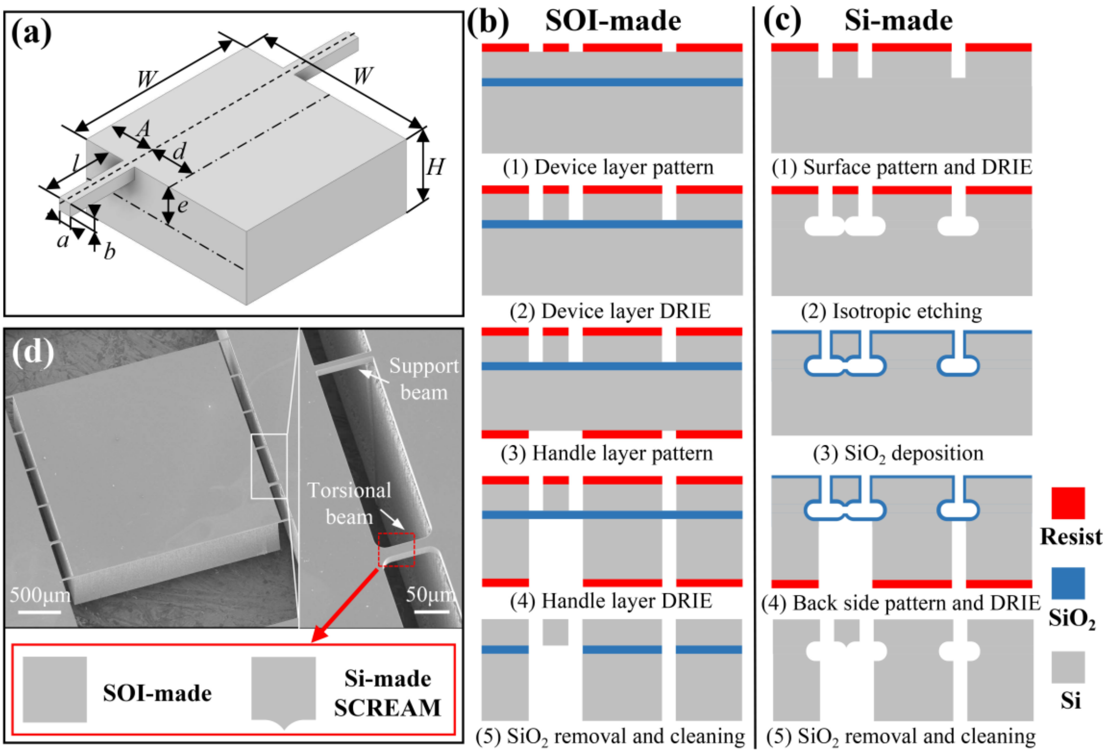

Figure 1

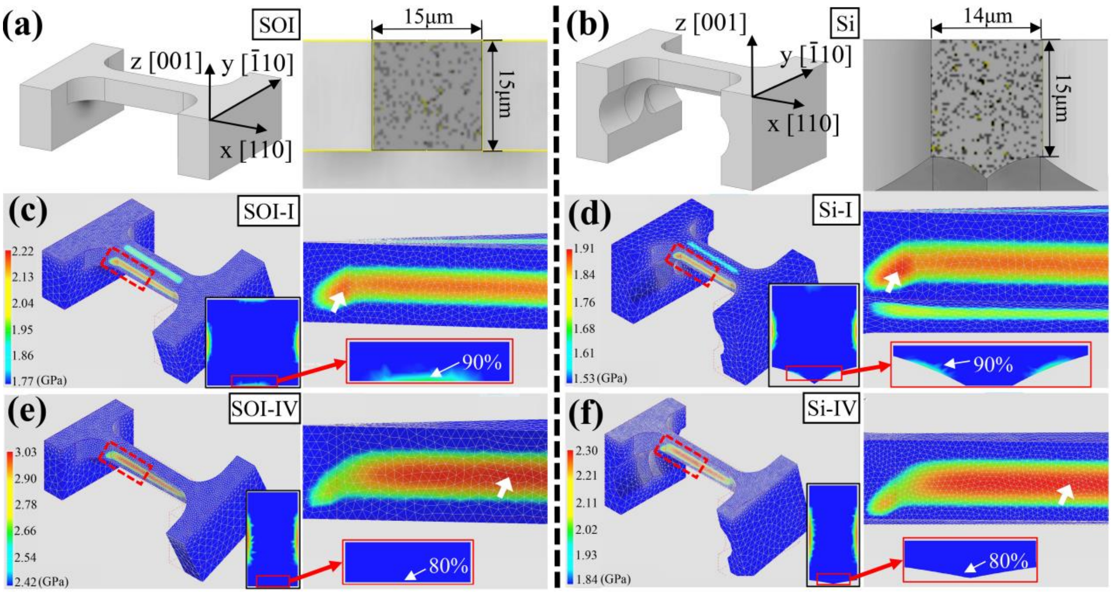

Figure 2

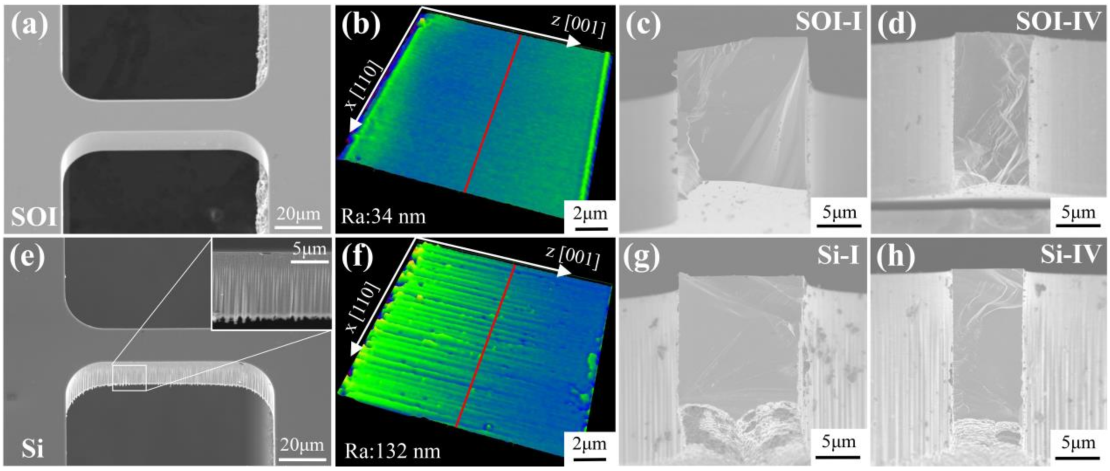

Figure 3

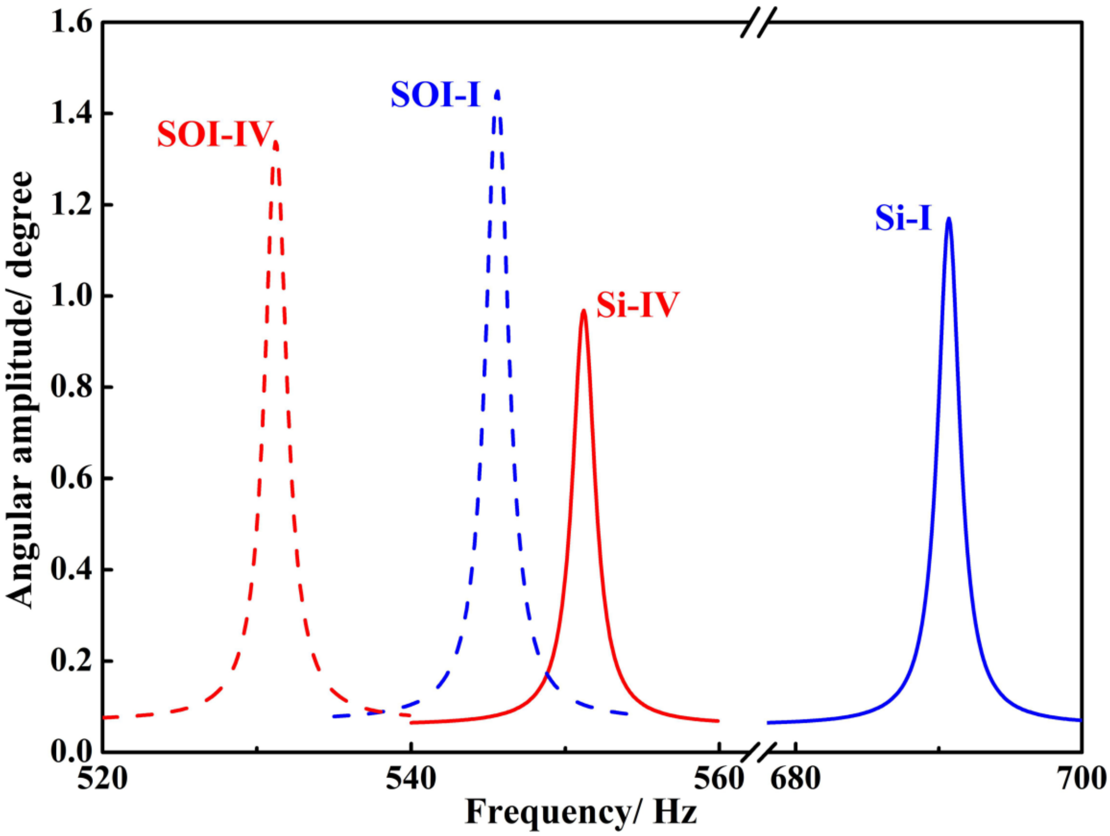

Figure 4

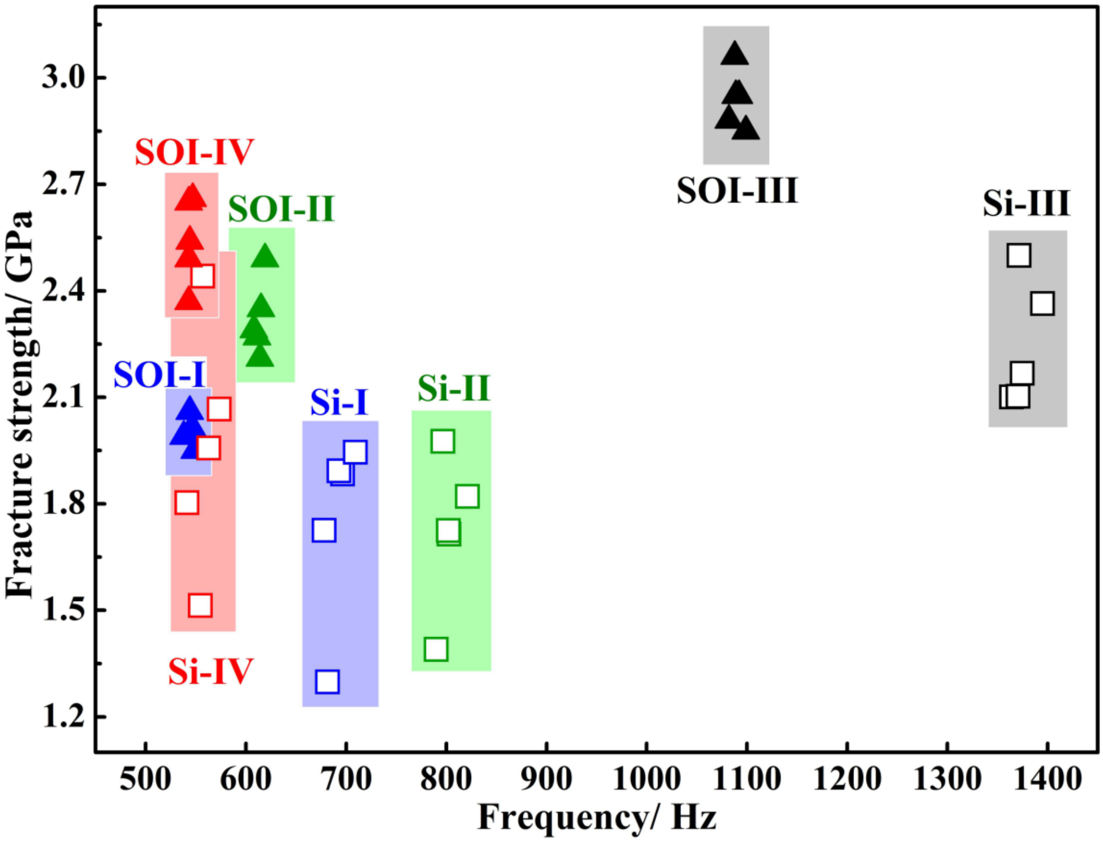

Figure 5

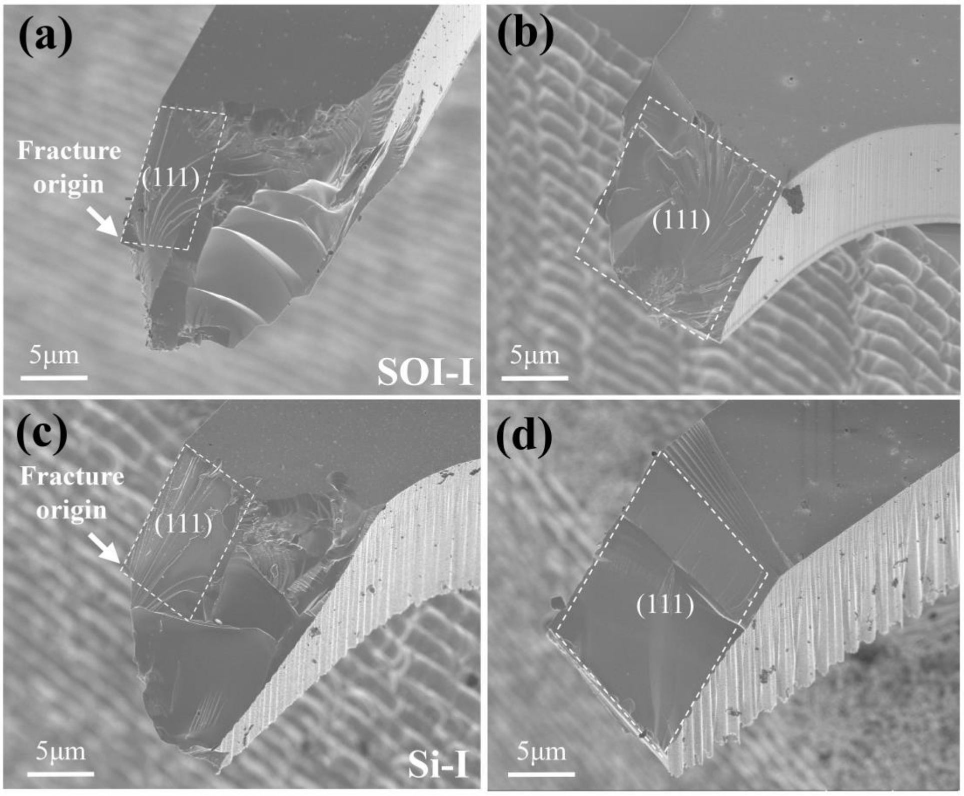

Figure 6

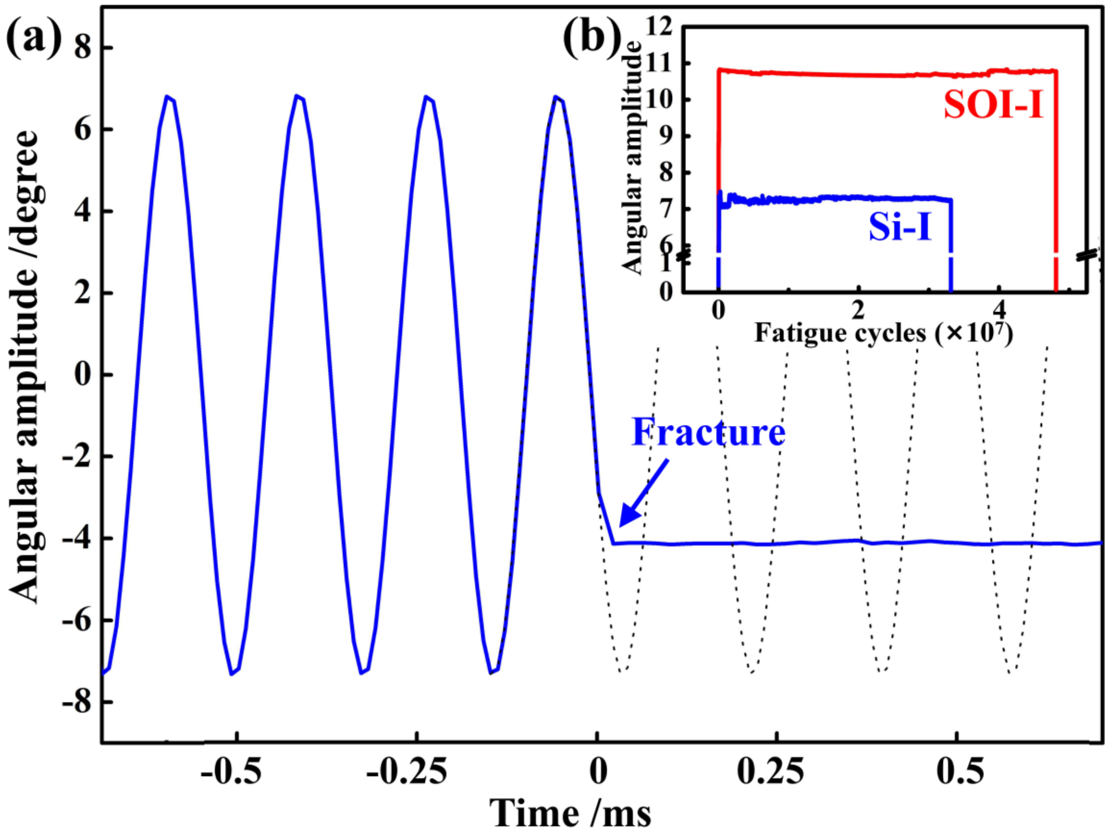

Figure 7

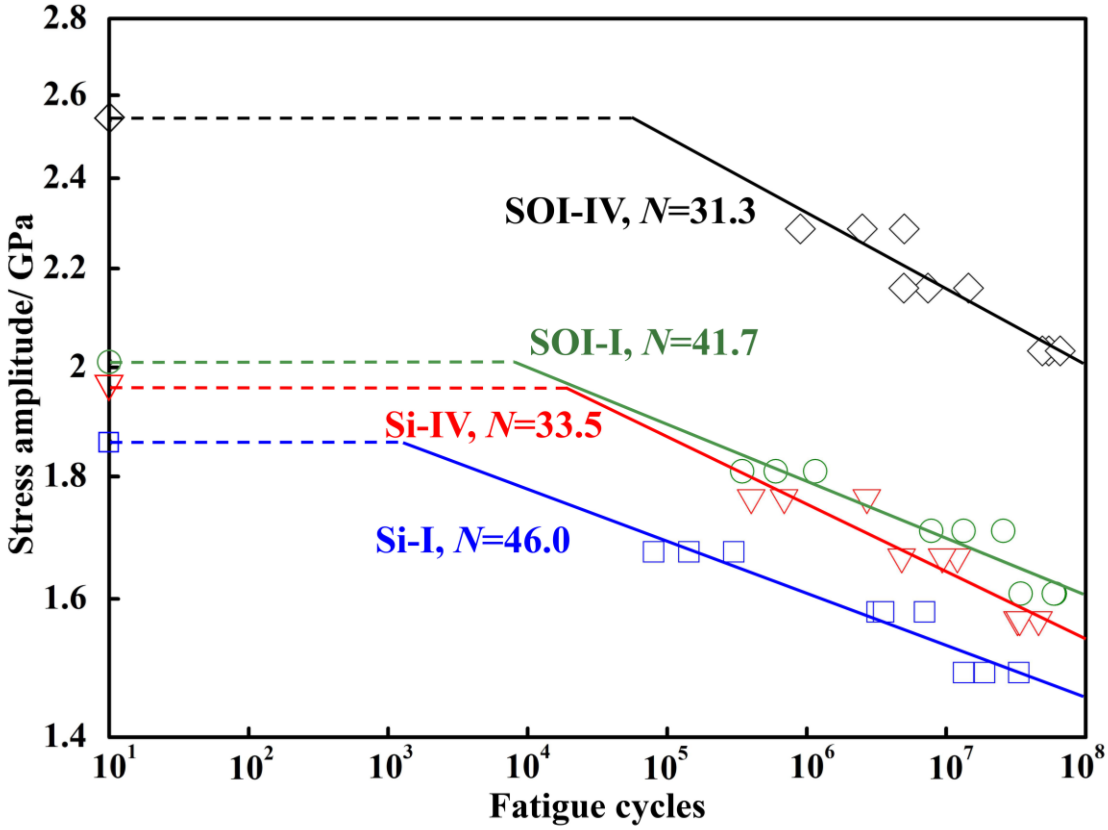

Figure 8